GEODYNAMICS
&
TECTONOPHYSICS

ГЕОДИНАМИКА
И
ТЕКТОНОФИЗИКА

2010. Vol. 1. № 1. 24–35

ISSN 2078-502X

PUBLISHED BY THE INSTITUTE OF THE EARTH'S CRUST

RESEARCH ARTICLE

Tectonophysics

EXPERIMENTAL STUDY OF THERMAL AND STRAIN FIELDS DURING DEFORMATION OF EN ENCHELON FAULTS AND ITS GEOLOGICAL IMPLICATIONS

Ma Jin[1], Ma Shaopeng[2], Liu Liqiang[1], Liu Peixun[1]

[1]*Institute of Geology, China Earthquake Administration, 100029, Beijing, China*

[2]*Beijing Institute of Technology, 100081, Beijing, China*

Abstract: The article presents results of experimental studies using a bi-axial servo-control system to apply load on samples with extensional and compressional en echelon faults. During the experiments, variations of temperature and thermal images were recorded synchronously by a multi-path contact-type thermometric apparatus and a thermal image system, respectively. A digital CCD camera was employed to synchronously collect images of specimens' surfaces. The digital speckle correlation method (DSCM) was utilized to analyze the images and to define displacements and strain fields. Our experimental results show that temperature fields have clear responses to opposite stress states in the jog areas of both types of the en echelon faults. Prior to failure of the jog area, its temperature is the highest at the compressional en echelon faults and the lowest at the extensional en echelon faults. Records by DSCM give evidence that mean strain of the jog area is the highest at compressional en echelon faults and the lowest at the extensional en echelon faults. It is revealed that deformation of the en echelon faults occurs in two stages, developing from stress build-up and fault propagation in the jog area to unstable sliding along the fault. Correspondingly, the mechanism of heating-up converts from strain heating into friction heating. During the period of transformation of the temperature rising mechanism, three events are observed in the jog area and its vicinity. Analyses of our experimental results demonstrate that variations of temperatures in the jog area can be indicative of fault sliding and suggest sliding directions. Observations and studies of temperature changes during transformation of the temperature rising mechanism at sensitive portions of faults are of great importance for early detection of precursors of unstable slip on active faults.

Keywords: En echelon faults (EEF), fault activity, temperature field, strain field, digital speckle correlation method (DSCM).

Recommended by *S.I. Sherman* 20 October 2009

Ma Jin, Ma Shaopeng, Liu Liqiang, Liu Peixun. Experimental study of thermal and strain fields during deformation of en enchelon faults and its geological implications // Geodynamics & Tectonophysics. 2010. V. 1. № 1. P. 24–35.

ЭКСПЕРИМЕНТАЛЬНОЕ ИЗУЧЕНИЕ ТЕПЛОВЫХ И ДЕФОРМАЦИОННЫХ ПОЛЕЙ В ПРОЦЕССЕ РАЗРУШЕНИЯ ЭШЕЛОНИРОВАННЫХ РАЗЛОМОВ И ИЗМЕНЕНИЯ ГЕОЛОГИЧЕСКИХ УСЛОВИЙ

Ма Цзинь[1], Ма Шаопхен[2], Лю Лицъянь[1], Лю Пхейксан[1]

[1]*Институт геологии, Китайская администрация по изучению землетрясений, 100029, Пекин, Китай*

[2]*Пекинский институт технологии, 100081, Пекин, Китай*

Аннотация: В статье представлены результаты экспериментального изучения эшелонированных разломов растяжения и сжатия с приложением нагрузки к двуосной автоматически регулируемой модели. В ходе эксперимента производились синхронные замеры температур и тепловых сигналов. Для этого были использованы, соответственно, многоканальный термометрический прибор контактного типа и система регистрации тепловых сигналов. Синхронные снимки поверхностей экспериментальных образцов были получены при помощи цифровой видеокамеры на основе устройства с зарядовой связью. Был применен цифровой метод спекл-корреляции (DSCM) для анализа снимков и определения смещений и деформационных полей. Была установлена очевидная реакция тепловых полей на состояния напряжения противоположных типов в зонах сочленения эшелонированных разломов обоих типов. Перед полным разрушением зоны сочленения самые высокие значения температуры зарегистрированы на эшелонированных разломах сжатия, самые низкие – на эшелонированных разломах растяжения. С помощью метода DSCM самые высокие значения среднего напряжения в зоне сочленения дислокаций зарегистрированы на эшелонированных разломах сжатия, самые низкие – на эшелонированных разломах растяжения. В процессе деформирования эшелонированных разломов выявлены две стадии, развивающиеся от накопления напряжений и прорастания разлома в зону сочленения дислокаций до неустойчивого скольжения по разлому. Соответственно трансформируется механизм нагревания – с нагревания напряжением до нагревания трением. В самой зоне сочленения дислокаций и поблизости от неё в процессе трансформирования механизма повышения температуры наблюдались три фазы. Анализ полученных нами экспериментальных данных показал, что вариации температуры в зоне сочленения дислокации могут указывать на смещения по разлому и позволяют предположить направление смещения. Наблюдение за изменениями температуры и их изучение в процессе трансформирования механизма повышения температуры на чувствительных отрезках разломов имеют большое значение в плане раннего выявления предвестников неустойчивого смещения по активным разломам.

Ключевые слова: эшелонированные разломы, активность разломов, тепловое поле, деформационное поле, цифровой метод спекл-корреляции (DSCM).

INTRODUCTION

In recent years, there have been many efforts of applying satellite observations to search for earthquake precursors, and scopes of studies of thermal anomalies associated with earthquakes and faulting are increasing [*Горький и др., 1988; Ouzounov, Freund, 2004; Morzova, 1997, 2000; Tronin, 1996; Tronin et al., 2002; Nusipov et al., 2003; Tramutoli V. et al., 2004; . Chen et al., 2003; Shan et al., 2005; Ma et al., 2000*]. In terms of physics, a relationship between thermal and strain fields during fault deformation is a basis for studying whether satellite data on thermal radiation and/or data on temperature fields observed on the ground can prove applicable to analyses of earthquakes and/or fault activity. Deformation by heating of metal has been studied quite well, while heating by deformation, particularly temperature variations caused by rock deformation, still needs to be more thoroughly studied. In the past decade, while discussing a potential relationship between satellite thermal infrared rates and data on earthquakes, heating by deformation and distribution of thermal fields produced by rock deformation has been paid more attention. Many authors have published results of laboratory observations of thermal radiation variations caused by deformation of rock specimens [*Lockner, Okubo, 1983; Cui et al., 1993; Deng et al., 1997; Dong et al., 2001; Geng et al., 1992; Geng et al., 1993; Wu, Wang, 1998; Liu et al., 2003; Qian et al., 2005; Yin et al., 2000; Wu et al., 2006; Wu et al., 2006; Freund, 2000; Freund, 2002; Freund, 2003; Freund et al., 2006*].

In our laboratory, we have performed experiments to synchronously record variations of temperature and thermal images by using a multi-path contact-type thermometric apparatus and a thermal image system at the frequency of 5Hz and a sampling rate of 12.5 frames per second, respectively. We observed that rates of thermal radiation «brightness» temperature T_B and temperature T varied synchronously with stress and acoustic emission under the condition of single-axis cycle loading [*Liu et al., 2004*]. Variations of T_B and T at the en echelon fault occurred synchronously with elastic deformation, stick-slip, and rupture of the fault under the condition of bi-axial loading; changes of temperature increase mechanisms at various deformation stages were also discussed [*Liu et al., 2007*]. It was noted that the temperature decrease was related with rupture spreading in the jog area, and the subsequent frictional slip can cause temperature rising [Ma *et al*., 2007]. In these studies, responses of thermal fields to strain fields have been preliminary researched.

The above conclusions have been mainly based on analyses of thermal image data which has low resolution and high background noise. To conduct a more through study of the relationship between the measured temperature field and the strain field and to review results of the previous experiments, we introduced two technical improvements in our experimental procedure. First, we use the digital speckle correlation method (hereinafter referred to as DSCM) to measure displacements and strain at all points on the specimen which is subject to self-heating, and heating spots are studied along with strain sensor points. Second, under the condition close to plane strain, we take measurements of strain and thermal radiation from the upper surface of the specimen, whereas measurements of temperature are obtained from the lower surface of the specimen, i.e. such measurements are taken independently and without any interference between each

other. In addition, we arrange more numerous points of temperature measurement in a denser pattern on the specimen in order to obtain more detailed information about variations of the temperature field and to ensure higher quality, precision and reliability of experimental data.

DSCM (also called digital image correlation method, DIC) is a technique applied in experimental solid mechanics to measure deformation fields [*Chu et al., 1985; Jin et al., 2002*]. In DSCM procedures, random spots on speckle images are regarded as carriers of deformation information; displacements of the points are traced in digital images by the grey scale matching in order to delineate a field of displacement. Then the displacement field is smoothed and differentiated numerically, yielding the strain field.

The measurement system to implement the DSCM procedures includes hardware and software [*Ma et al., 2006*]. The hardware records speckle images and other useful information on the surface of the specimen during loading, and the software analyzes the images to obtain data on displacement and strain fields. Before the DSCM measurements, the surface of a specimen usually needs to be sprayed with a special fluid to produce a pattern of random speckles. In our experiment, a rock specimen of granodiorite has a natural speckle pattern on its surface due to differences in colours of its mineral grains. Therefore, we have taken advantages of using a digital CCD camera to directly obtain numerical images of the specimen's surface. All the measurements in this experiment have been adjusted to the time of loading to maintain the simultaneity of variations of physical data.

In view that the thermal image system has its inherent background distortion and zero drift, results of analyses of the thermal images and temperatures were compared and discussed in the previous publications [*Liu et al., 2007; Ma et al., 2007*]. This study is focused on analysing the data on temperature, which have fairly good resolution and stability, partial displacement and strain fields. Our main objective is to study temperature variations caused by deformation of the en echelon faults.

EXPERIMENT DESIGN AND PROCEDURES

En echelon faults (hereinafter referred to as EEF) are among most commonly observed fault structures in nature. As jog areas of extensional and compressional EEF have opposite stress states, comparing their thermal and strain fields can provide characteristic implications for identifying orientations of fault slip. In our experimental study, we consider two types of EEF as objects for simulation. Two samples of granodiorite, 500 mm × 300 mm × 50 mm in size, were obtained in the Fangshan county of Beijing. Each sample is cut at an angle of 31° to the longitudinal axis Y in an en echelon manner. The produced cuts are filled with gypsum to simulate faults of low strength. The specimens with structures of extensional and compressive EEF and an area subject to the DSCM observation are schematically shown Figures 1, *a* and *b*. To detect variations of temperatures parallel and across the faults and the jog area, 32 temperature measurement points are arranged on each specimen within the jog area and located parallel (Fr-P, Fl-P) to and across (Fr-A, Fl-A) the faults (see Fig. 1).

The experiments are performed on a biaxial servo-control loading system. A constant pressure is imposed to the rock specimen in the X direction. Stresses in the X direction amount to 5 MPa, 6 MPa, and 7 MPa in three successive stage of stick slipping, respectively. In the Y direction, a constant displacement rate is maintained (0.5 μm/s).

Displacement and strain fields on the upper surface of the specimens are observed by DSCM in the areas shown as dotted boxes in Figure 1. The resolution of displacement measurements by DSCM depends on sizing of pixels in the digital images recorded by the hardware system. To enhance the resolution of displacement measurements, only the most important part of the specimen' surface is subject to observation. The temperature measurement points are arranged on the lower surface of the specimen, their locations being shown respectively on the upper surface along with measurement points for DSCM (see Fig. 1). The resolution of the platinum resistance thermometer is 2.053 mk/numeral with deviation ±1 numeral. All the measurements are conducted synchronously.

For comparative analyses, experimental data are processed as described below.

A rate of the differential stress is calculated as follows:

$$Dy = Px - Py\ ,$$

wherein Dy is the differential stress, Py and Px are stresses in the Y and X directions, respectively. At the moment of Py=Px, i.e. the differential stress is zero, the temperature is set at zero. Then other temperatures are set up, so that variations of the temperature with changes of the differential stress become more pronounced.

Temperatures at the points, which are not subject to any impact and located far away from the portions under stress concentration, are taken as background temperatures for adjustment of temperature measurement records. The background temperatures are subtracted from the recorded data to estimate relative variations of temperatures at all the points. The temperature rates of all the measurement points are then converted into centigrade degrees, and adjusted stepwise for every set of 50 measurements to remove noise.

After processing, effects of the background temperature and variable environment are eliminated from the temperature measurement records, yielding relative variations of temperatures at all points on the specimen that are caused by deformation.

EXPERIMENTAL RESULTS

Temperature variations in the jog area

Figure 2 shows variations of temperature in the jog area and differential stress Dy that are observed in

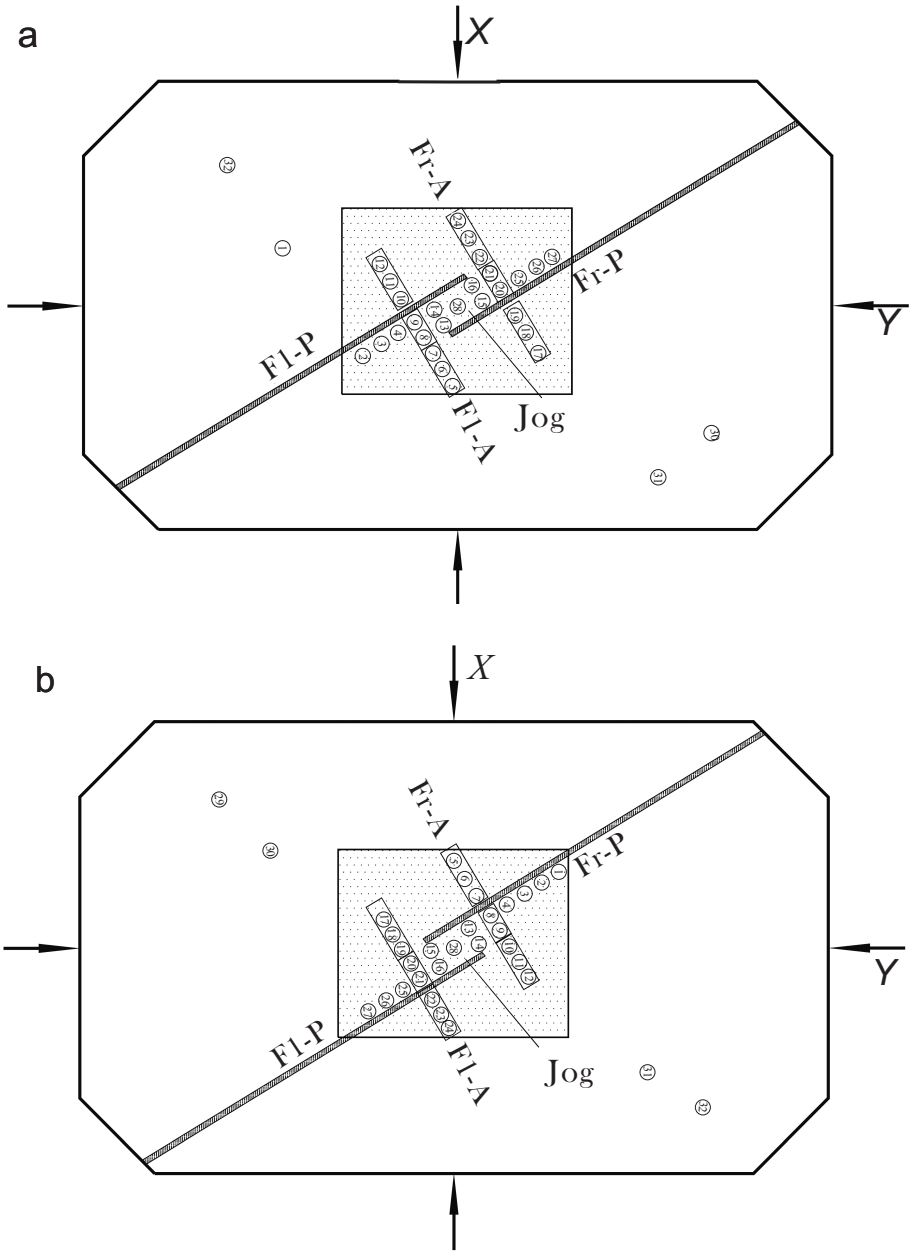

Fig. 1. Schemes of specimens cut by extensional (a) and compressional (b) en echelon fault structures.
The left fault, Fl and the right fault, Fr are shown by thick lines. Circles with numbers show positions of temperature measurement points. 'Jog' denotes the jog area of the en echelon fault. Fl-A and Fr-A are measurement lines across the left and right faults, respectively. Fl-P and Fr-P are measurement lines parallel to the left and right faults, respectively. The dotted box shows the area studied by DSCM.

Рис. 1. Схемы образцов, рассеченных эшелонированными разломными структурами растяжения (*a*) и сжатия (*b*).
Левосторонний разлом (Fl) и правосторонний разлом (Fr) показаны широкими линиями. Кружки с номерами показывают расположение точек замера температуры. Участок, обозначенный словом «Jog», показывает зону сочленения эшелонированного разлома. Fl-A и Fr-A – линии замеров поперек левостороннего и правостороннего разломов, соответственно. Fl-P и Fr-P – линии замеров параллельно левостороннему и правостороннему разломам, соответственно. Участок, изученный с применением метода DSCM, помечен точечной штриховкой.

experiments with the specimens cut by the extensional and compressional EEF. For both types of EEF, deformation takes place in two stages, i.e. complete breakdown of the jog area and stick slipping under low, medium and high normal stress. In the experiment with the specimen cut by the extensional EEF, stick slipping occurs after the jog area gets completely destroyed (Fig. 2, *a*). In the experiment with the specimen cut by the compressional EEF, the process of deformation lasts for quite a long time before the jog area gets completely destroyed, and numerous events of stick-slip occur under low normal stresses, while the temperature rates are much higher than the initial temperature value (Fig. 2, *b*).

It is observed (Fig. 2, *a*) that failure of the jog area at the extensional EEF occurs at low stress, i.e. around

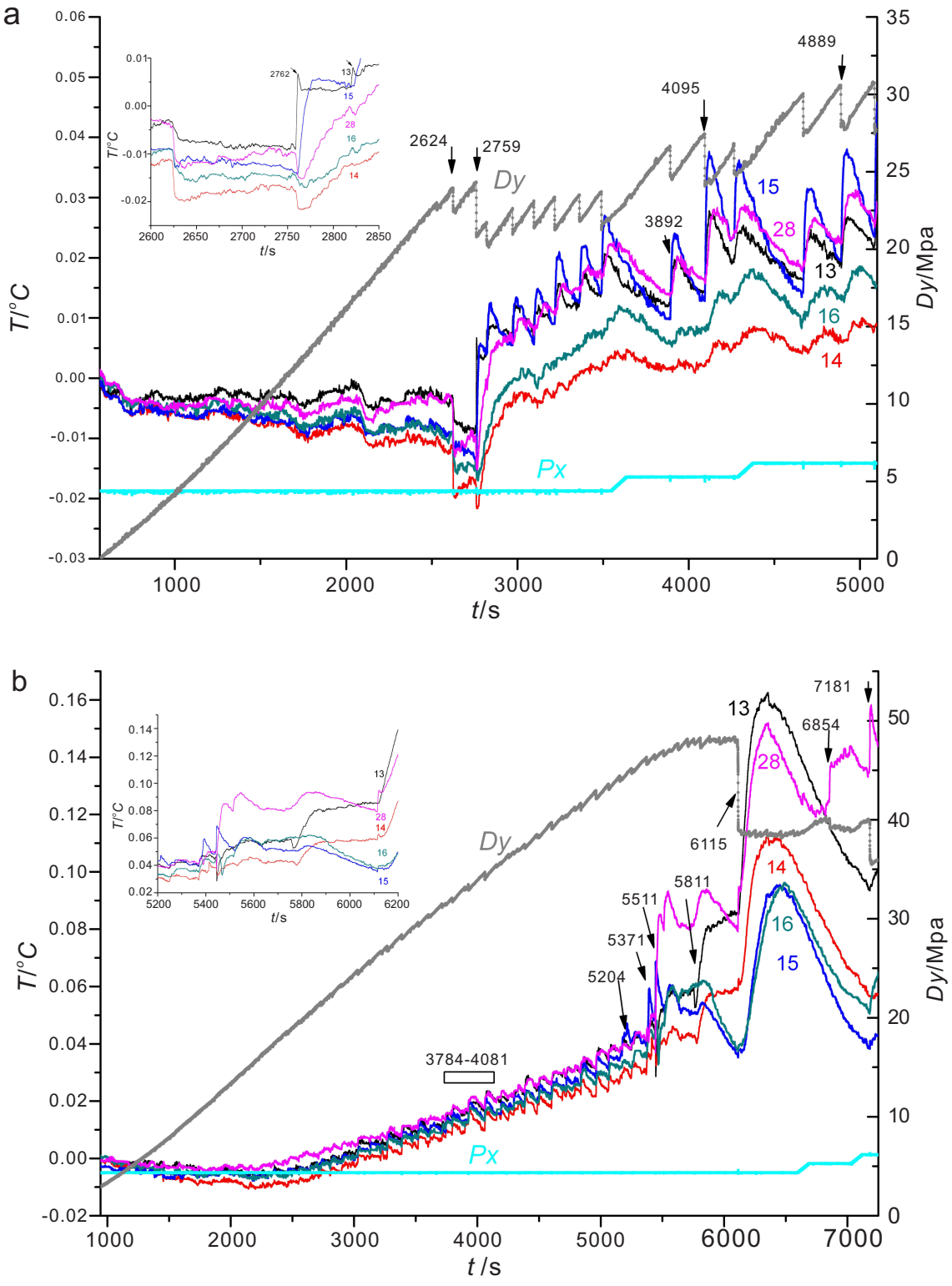

Fig. 2. Variations of temperatures in the jog area and differential stress Dy in experiments with the specimens cut by extensional (*a*) and compressional (*b*) en echelon fault structures.
Coloured curves show temperatures at the measurement points which are marked by numbers of the same colours as the curves. Dy is the differential stress, and Px is the stress in the x direction, plotted by the dark grey and cyan curves, respectively. Black numerals with down-pointed arrows above curves correspond to timing of events described in the text. The upper left inset shows magnified temperature variations at the moment of complete failure of the jog area between the faults.

Рис. 2. Вариации температуры в зоне сочленения дислокаций и дифференциальных напряжений (Dy) в экспериментах на образцах, рассеченных эшелонированными разломными структурами растяжения (*a*) и сжатия (*b*).
Цветные кривые показывают температуры в точках замера, помеченных номерами того же цвета, что и кривые. Dy – дифференциальное напряжение (кривая темно-серого цвета); Px – напряжение в направлении x (кривая бирюзового цвета). Номера в направленных вниз стрелках над кривыми показывают время событий, описываемых в статье. Врезка вверху слева показывает вариации температуры на момент полного разрешения зоны сочленения между разломами.

24MPa. The stress drops twice, at 2.624 sec and 2.759 sec, with changes of the temperature which decreases at 2.624 sec and increases at 2.759 sec, as shown in a concave curve in Figure 2, *a*. At 2.624 sec, abrupt temperature drop occurs at all the measurement points in the jog area, and the drop is most pronounced at points 14 and 16 on the left fault, which implies tensile deformation start-up and rupture in the jog area. At 2.759 sec, the temperature rises suddenly at points 13 and 15 near the right fault, wherein a considerable decrease of the temperature has been recorded before. Meanwhile, at measurement points 14 and 16 close to the left fault and at point 28 in the middle of the jog area, the temperature drops first and rises afterwards, yet at a smaller rate with an evident time lag, which means that sliding occurs first at the right fault. It is interesting that temperature pulses occur at point 13 before temperature rising at all other points (see the upper left diagram in Fig. 2, *a*). This phenomenon occurs many times prior to the ensuing stick-slip events.

At the compressional EEF (Fig. 2, *b*), the temperature of the jog area increases gradually with enhancing deformation, and a large stress drop occurs at 6.115 sec, accompanied with failure of the jog area at a high stress of around 45 MPa. During the failure of the jog (5.511–6.115 sec), the temperature raises three times stepwise (Fig. 2, *b*). Before the first event (5.511 sec), several small events occur, including two events of temperature rising pulses at point 15 near the tip of the right fault, then extending toward points 13 and 28. In the second event (5.811 sec), relatively slight variations of the temperature are recorded. The third event of temperature rising (6.115 sec) is the most pronounced. During this event, the temperature rises at point 13 to the largest rate; at points 15, 16, and 28, the temperature drops first and then considerably rises. With these three events of temperature variations, the jog area starts to rupture from its right portion, then toward its left portion under the process of failure is complete.

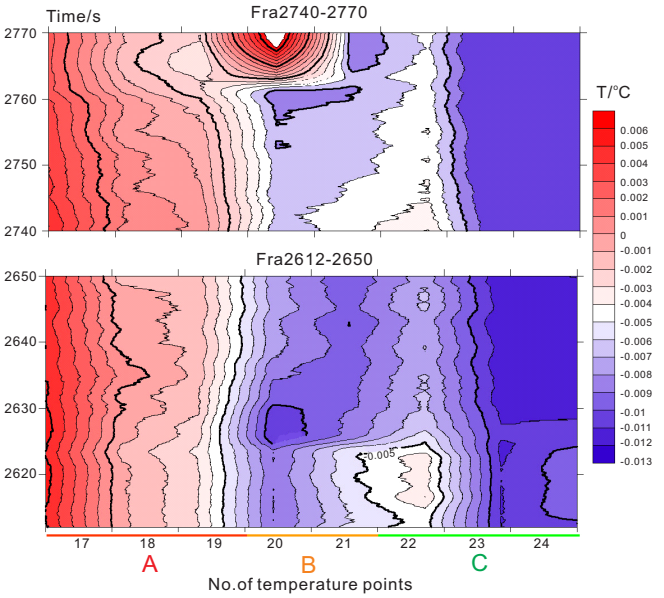

Fig. 3. Temperature variation along profile Fr-A across the right fault during fracturing at the jog of the extensional en echelon structure. Along the abscissa, positions of measurement points from 17 through 24 (see Fig. 1, *a*) and sections A, B, and C are shown. The ordinate shows timing (two unstable slip events at 2.624 sec and 2.759 sec). Contours denote temperature distribution.

Рис. 3. Вариации температуры вдоль профиля Fr-A, пересекающего правосторонний разлом, в процессе разломообразования в зоне сочленения дислокации эшелонированной структуры растяжения.
На оси абсцисс показаны места расположения точек замера № 17–24 (см. рис. 1, *a*) и участки A, B и C. На оси ординат показано время (два смещения на 2624 с и 2759 с). Распределение температуры оконтурено.

Temperature variations across the faults

As shown in Figure 1, profiles Fr-A and Fl-A are two measurement lines crossing both the right fault and the left fault of the en echelon structures, respectively. Our study to illustrate temperature variations with time is focused on the right fault, as an example. Figure 3 shows temperature variations with time and location at the measurement lines across the right fault in the en echelon structure around two unstable slip events. Taking into account that the total experimental time span is relatively long, and variations during the period from 2.650 sec through 2.740 sec are recorded as insignificant, this episode is omitted in Figure 3. It is noted that the temperature change can be divided into three sections: A, B and C. Section B (points 20 and 21 in the jog area) shows a concave-shape process with a significant temperature drop at 2.624 sec, while temperature rising at points 19 and 20 (the right fault located between them) is most pronounced at 2.759 sec. In section C (points 22, 23, and 24), temperature variations are similar to those in section B, though more gentle. The process of temperature variations in section A (points 17, 18, and 19) is opposite to that in sections B and C. While the temperature drops in B and C, it rises in A, and, *vice versa*, as temperature rises in B and C, it drops in A. Before the unstable slip event at 2.759 sec, the temperature of the jog area is the lowest. Between points 19 and 20, the temperature rates are the highest before the unstable slip event, afterwards the temperature rises to the maximum.

During breakdown of the jog area, temperatures vary with time across the right fault of the compressional en echelon structure. In the process of temperature rising, three events are distinguished in the jog area (see Fig. 2, *b*).

Figure 4 shows temperature variations at the measurement points across the right fault around the third event which occurs at 6.115 sec. It is the strongest event characterised by a considerable temperature rise at the right fault (between points 7 and 8). It illustrates that before the moment of 6.115 sec, the temperatures is the highest at point 8 (inside the jog area), and temperature rising at the fault does not happen until the temperature pulse with an abrupt increase occurs at point 8. This fact suggests that the temperature increase at point 8 triggers unstable slip of the fault.

Our studies give grounds to make the following conclusions regarding temperature changes across the faults in the two types of EEF structures: (1) The pro-

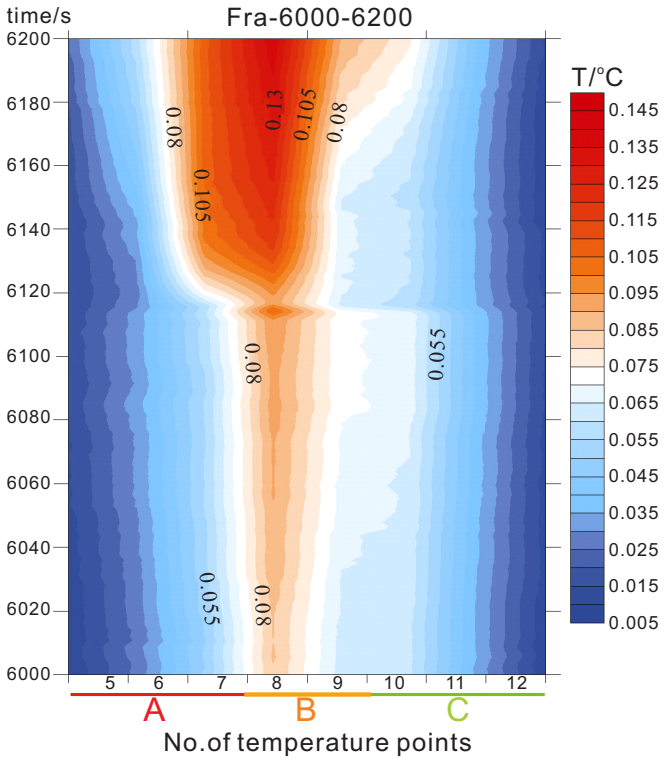

Fig. 4. Temperature variations along profile Fr-A across the right fault of the compressive en echelon structure around the third unstable slip at 6.115 sec.
Along the abscissa, positions of measurement points from 5 through 12 (see Fig. 1, *b*) and sections A, B, and C are shown. The ordinate shows timing. Contours show temperature distribution.

Рис. 4. Вариации температуры вдоль профиля Fr-A, пересекающего правосторонний разлом, в процессе разломообразования в зоне сочленения дислокации эшелонированной структуры сжатия с приближением третьего смещения на 6115 секунде.
На оси абсцисс показаны места расположения точек замера № 5–12 (см. рис. 1, *b*) и участки A, B и C. На оси ординат показано время. Распределение температуры оконтурено.

cess of temperature variations in the jog area is more complicated than that in the sections on its two sides. In the jog area of the extensional EEF structures, the temperature is the lowest. It is the highest in the jog area of the compressional EEF structures. (2) When the jog area breaks down completely, the temperature rises abruptly on the sliding fault. (3) Temperature pulses, i.e. rapid rising and dropping in an instant, often occur near the fault tip prior to unstable slip.

Temperature variations parallel to the faults

As described above, on the inner side of the jog area in the extensional and compressional EEF structures, two measurement lines are arranged sub-parallel to the faults (see Fr-P and Fl-P, respectively, on Fig. 1). In this article, we describe Fr-P in detail as a case study. The measurement points are aligned from the jog area to the middle of the right fault (see Fig. 1). Two sections are distinguished, section A close to the jog area, and section B far from the jog area.

Figure 5 displays temperature variations on Fr-P of the extensional EEF during two unstable events. The process is similar to that shown in Figure 3 (with the episode of 2.650–2.740 sec being omitted). It suggests that the event at 2.624 sec makes the temperature to decrease synchronously near the right fault. Fast fluctuations occur before temperature dropping (2.615 sec) at measurement points 15 and 20 close to the jog area. Near the second event, the temperature rises first at points 13 and 8 near the tip of the right fault, also close to the jog area. About five seconds later, the temperature increases at others points along Fr-P. During the failure of the jog area (the first event), temperature variations are more complicated in section A, and the rising amplitude of temperature during the second event is larger in section B.

Figure 6, showing the compressional EEF structure, illustrates temperature variations with time along Fr-P during the first and the third events shown in Figure 2, *b*. During the first event (see Fig. 6, *a*), the temperature rises dominantly at point 15 near the tip of right fault. Then temperature is subject to large lateral variations along the fault. During the third event, temperature pulses occur at points 4 and 8 near the tip of the left fault, and then the temperature rises gradually at the

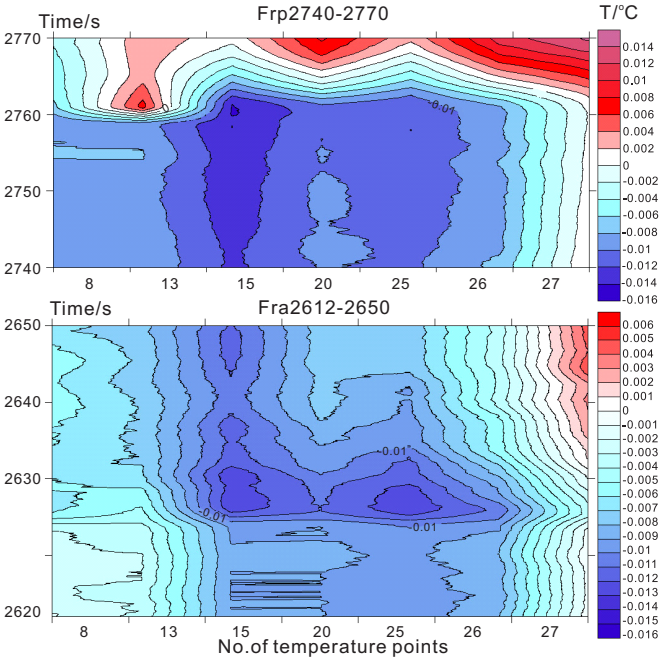

Fig. 5. Temperature variations parallel to the right fault during fracturing in the jog area of the extensional en echelon structure.
Along the abscissa, positions of measurement points along Fr-P from under left to upper right are shown (see Fig. 1, *a*). The ordinate shows timing (two unstable slip events at 2.624 s and 2.759 s). Contours show temperature distribution.

Рис. 5. Вариации температуры параллельно правостороннему разлому в процессе разломообразования в зоне сочленения эшелонированной структуры растяжения.
На оси абсцисс показаны места расположения точек замера вдоль профиля Fr-P в направлении снизу слева направо вверх (см. рис. 1, *a*). На оси ординат показано время (два смещения на 2624 с и 2759 с). Распределение температуры оконтурено.

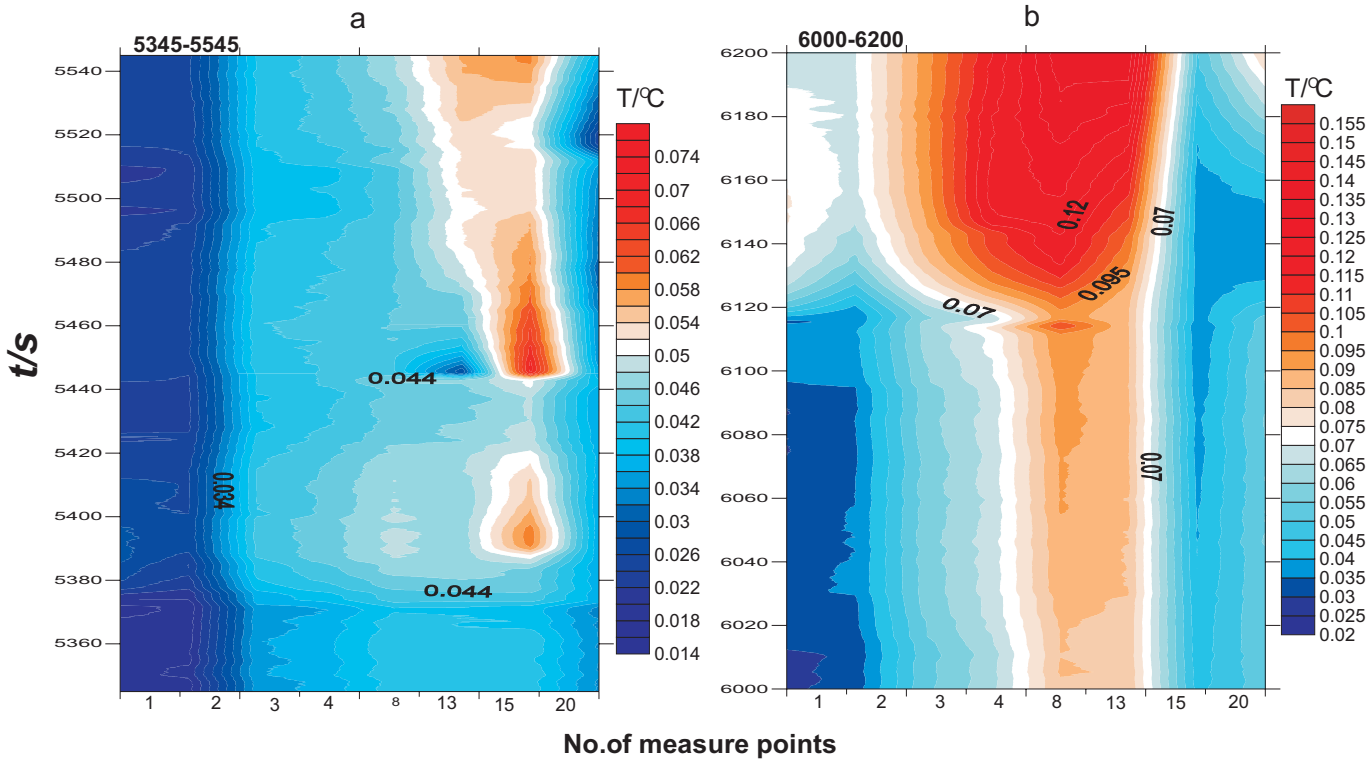

Fig. 6. Temperature distributions along Fr-P during fracturing of the jog area of the compressive en echelon structure.
Along the abscissa, relative positions of measurement points from the jog area (right) to the fault (left) are shown. The ordinate shows timing. (*a*) 5.345 sec – 5.545 sec; (*b*) 6.000 sec – 6.200 sec.

Рис. 6. Распределение температуры параллельно профилю Fr-P в процессе разломообразования в зоне сочленения эшелонированной структуры сжатия.
На оси абсцисс показаны места расположения точек замера от зоны сочленения (справа) до разлома (слева). На оси ординат показано время: (a) 5345–5545 с; (b) 6000–6200 с.

other points along the right fault (see Fig. 6, *b*).

It can be concluded that (1) the temperature variations along Fr-P of the two types of EEF structures during breakdown of the jog area are more complicated in section A than in section B during fracturing of the jog area; (2) the temperature pulses usually occur before the instable events.

Pulse of temperature rising and its implications

The pulse of temperature rising mentioned above is a phenomenon which has been observed in our experimental study after measurement points were arranged in a denser pattern on the specimens, as shown in Figures 2, *a*, 4, 5 and 6, *b*. These pulses occur near one of the fault tip and are manifested by rapid rise and fast drop of the temperature. Since stress growth can generate temperature rising and stress release can cause temperature dropping, the phenomenon of the temperature rising pulse is presumably associated with singular stress concentration at the fault tip and stress release caused by rupture spreading.

Figure 7 illustrates temperature distributions on the extensional en echelon faults at four moments, from which we infer the relationship between temperature pulses and fault slip. At 2.762 sec, the temperature is relatively high at point 13, which is very close to the tip of the right fault, on the background of low temperature (Fig. 7, *a*), actually presenting a small pulse shown in the inserted magnified diagram in the upper left corner of Figure 2, *a*, where the arrows indicate a temperature pulse at point 13 before temperature rising of all points on the right fault of the EEF structure. Then at 2.783 sec, the temperature along the right fault rises abruptly, forming a zone of high temperature (Fig. 7, *b*). It means that the rupture spreading of point 13 drives slip of the right fault. At 3.892 sec, the temperature increases relatively at point 13, while there is no zone of temperature variations on the fault (Fig. 7, *c*). Afterwards, at 3.914 sec, the temperature rises at all points on the right fault, generating a zone of high temperature (Fig. 7, *d*). It implies that propagation of the fault tip is the condition for unstable slip of the fault. The pulse of temperature rising occurs 10–20 sec prior to large slip, thus temperature rising at the fault tip is probably a precursor to unstable slip of a fault.

Comparison of thermal field and strain fields caused by deformation of en echelon structure

For a set of en echelon faults, complete breakdown of the jog area is an essential condition of sliding along

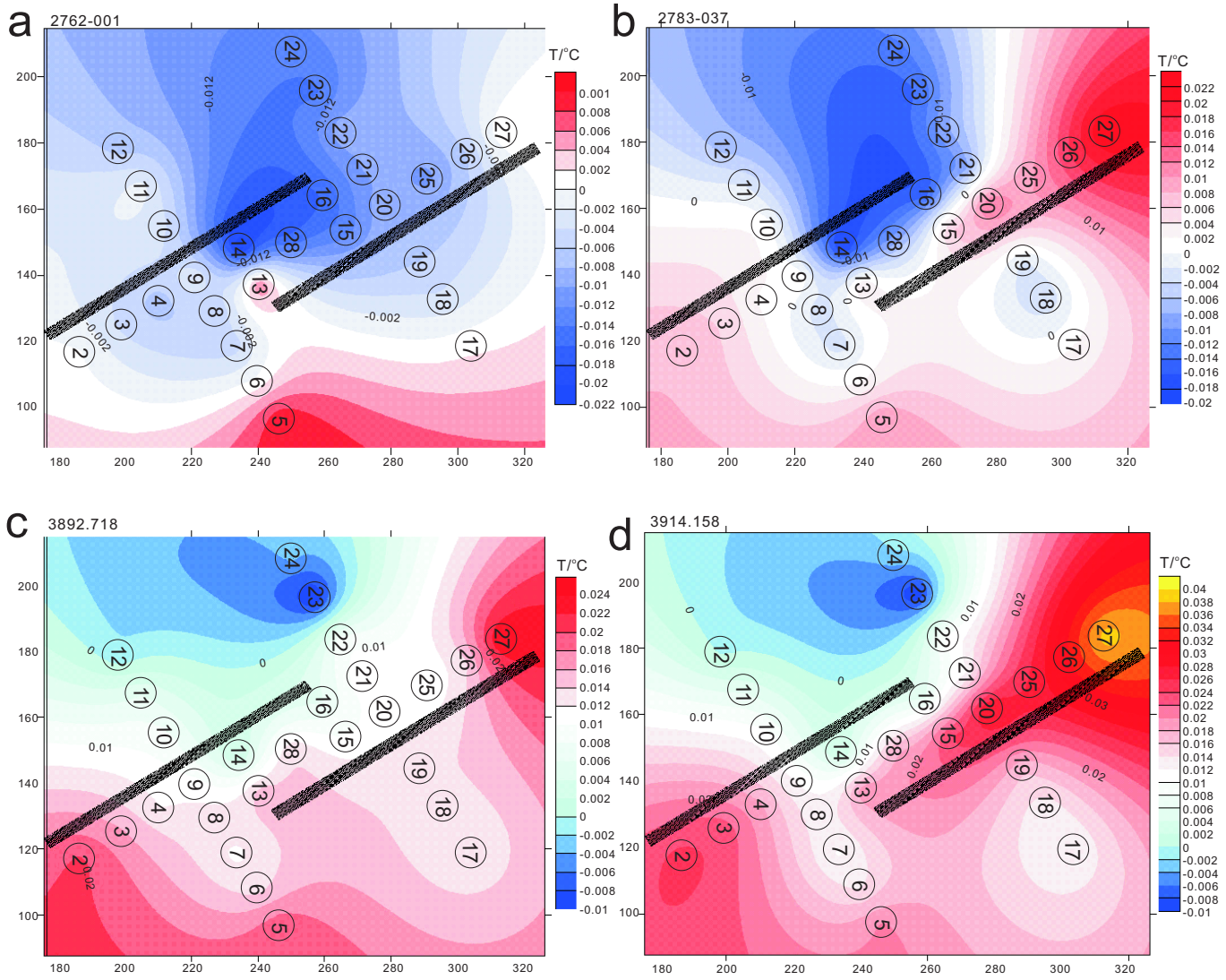

Fig. 7. Correlation of temperature rising pulses and fault slip: (*a*) 2.762 sec; (*b*) 2.783 sec; (*c*) 3.892 sec; (*d*) 3.914 sec.

Рис. 7. Корреляция импульсов подъема температуры и смещения по разлому: (*a*) 2762 с; (*b*) 2783 с; (*c*) 3892 с; (*d*) 3914 с.

faults. In this view, the jog area is a portion which is sensitive to fault sliding. Under the loading conditions shown in Figure 1, the jog areas of the compressive EEF are subject to compression, and the jog areas of extensional EEF are subject to extension. Prior to failure of the jog area, its temperature is decreasing with increasing stress (see Fig. 2, *a*). As shown in Figure 8a, when approaching the failure (at 2.612 sec), the temperature is low and has negative values in the jog area; it is high outside the jog area on the EEF. On the contrary, the temperature is high in the compressive jog area and low outside the jog area on the specimen (Fig. 8, *b*), when breakdown of its jog is impending (at 5.371 sec), and the temperature of the jog area is rising with stress growth.

Figures 8, *c*, and 8, *d*, illustrate displacements in Y direction (toward right is positive) on the extensional and compressive EEF at a moment during stable deformation revealed by DSCM. They indicate that all points are displaced leftwards (negative values), and the displacement field is cut into different domains by two faults shown. On the specimen of the extensional EEF, the jog area between the left and right faults has small displacements and big intervals of displacement contours, whereas displacements are large at the outer sides of the faults, and contour intervals are small. It implies that the outer sides of the two faults are compressed in Y direction and the jog area is relatively extended. On the contrary, on the specimen of the compressive EEF, the displacement contours in the jog area are more closely spaced than those at the outer sides of the two faults, indicating relative compression of the jog area. The mean strain fields (compressive strain is positive) prior to failure of jog areas on the extensional and compressive EEF specimens are shown in Figures 8e and 8f, respectively. It can be seen that on the extensional EEF the mean strain in the jog area is lower than that of surroundings, while on the com-

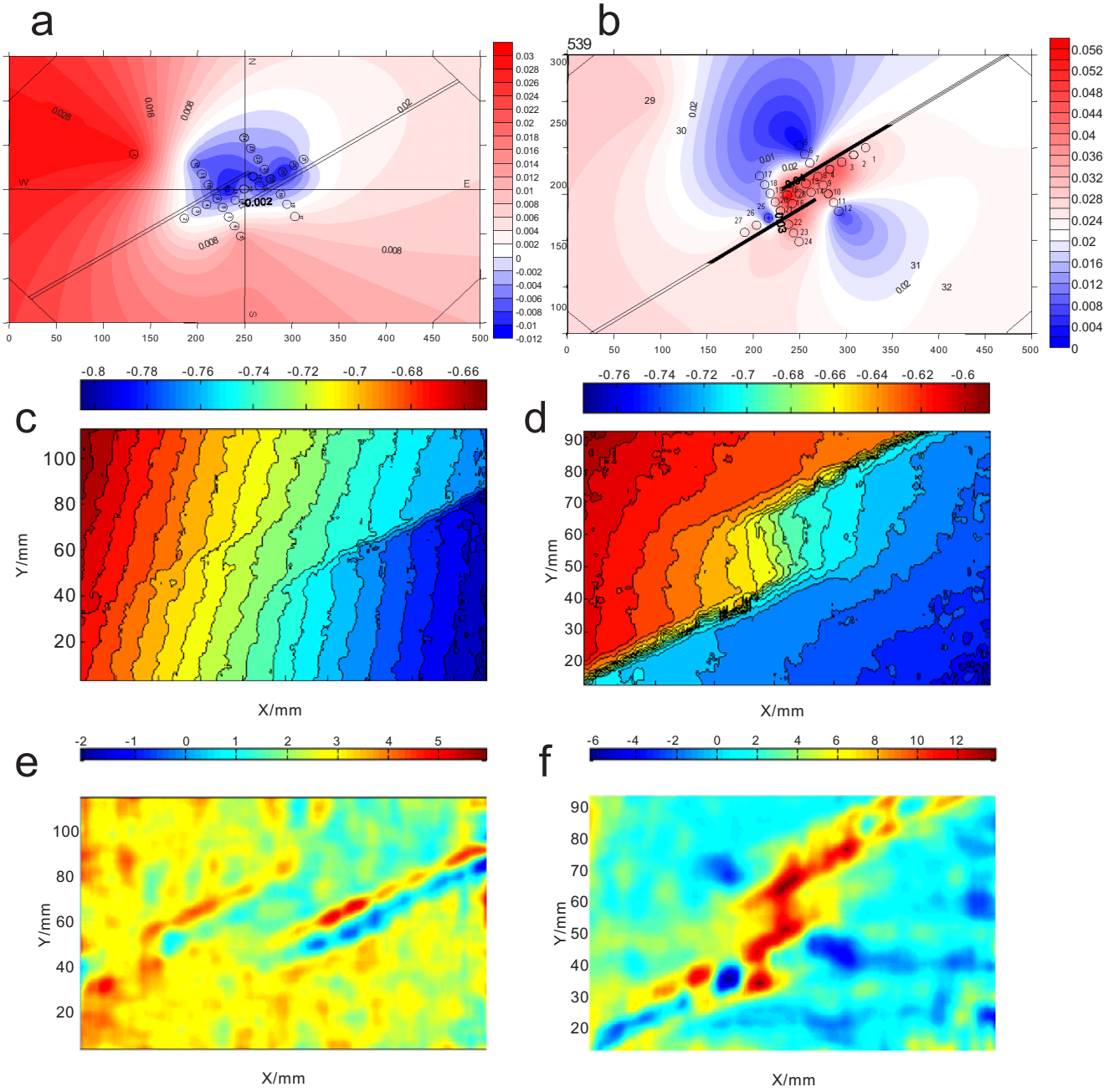

Fig. 8. Measurements of physical fields of the en echelon fault specimens prior to breakdown of the jog area: (*a*) and (*b*) are temperature contours; (*c*) and (*d*) are displacements in the Y direction (towards right is positive); (*e*) and (*f*) are mean strain; (*a*), (*c*), and (*e*) are for the extensional EEF; (*b*), (*d*), and (*f*) are for the compressional EEF.

Рис. 8. Замеры физических полей на образцах с эшелонированными разломами до разрушения зоны сочленения дислокации. (*a*) и (*b*) – температурные контуры; (*c*) и (*d*) – смещения в направлении Y (положительные в направлении направо); (*e*) и (*f*) – среднее напряжение; (*a*), (*c*) и (*e*) – для структур растяжения; (*b*), (*d*) и (*f*) – для структур сжатия.

pressive EEF the average strain in the jog area is higher than that of surroundings. Furthermore, in the extensional en echelon case, the range of mean strain is small (-2~+6 × 10^{-4}), while in the compressive en echelon case it is large (-6 ~ +13 × 10^{-4}). Variations of the thermal and strain fields reflect differences of strain state on the both sides of the fault as well as the processes of temperature rising by compression and temperature declining by extension. The result is in agreement with the statement of the thermodynamics on the relationship between material deformation and temperature change under heating dilatation, i.e. the temperature ascends with increasing pressure and descends with decreasing pressure, and the temperature is raised by compression and lowered by extension [Xie, 1980].

The above described experiments suggest that, as the scalar variable, temperature is sensitive to deformation.

CONCLUSIONS

Comparison between extensional and compressive EEF

On the extensional EEF, during failure of the jog area, temperature variations occur in two processes, temperature dropping and temperature rising. When temperatures decrease, the jog area starts to break; when temperatures increase, the jog area breaks down completely, and fault sliding occurs. On the compressive EEF, during failure of the jog area, the temperature rises stepwise. In the compressive case, the amplitude of temperature variations is up to 170 mK (rising 130 mK during failure), while it is merely 50 mk in the extensional case (20–30 mk during failure). In the compressional case, the temperature of the jog area is the highest before its failure. On the contrary, in the extensional case, the temperature of the jog area is the lowest before failure. The results of studies by DSCM show that the jog area of the compressional EEF has the largest mean strain, while the jog area of the extensional EEF has the smallest mean strain, corresponding to the relationship of temperature changes with strain change described above. These differences can be useful for determining slide manners of en echelon faults in the field.

Features and mechanism of temperature variations

On the EEF, during failure of the jog area, the temperature undergoes complicated variations, then drops first in the jog area and rises afterwards on the faults. The boundary of these two processes in time is very distinct. The temperature variation is related with extension or compression of the jog area and its rupture propagating, and the latter temperature rising is associated with frictional slip on the faults. Two mechanisms generate different variations of temperature. Temperature variations caused by strain (without rupture) are small. At the early stage of deformation on the EEF (even if there is singular stress concentration at the fault tip), temperature change by strain is less than 0.01ºC, while temperature variations caused by friction slip are several times this value. The temperature variations by early strain are slow, and distributed in planar or point manners, while those produced by frictional slip of faults exhibit a linear distribution.

The jog area is the most favourable portion to detect instability anomalies along a fault

Around instability, the mechanism of temperature variations is transformed near the jog area, i.e. from strain-related change to friction-related change. There are three kinds of thermal field anomalies: (1) temperature dropping with breakdown of the jog area, that is followed by temperature rising with fault pre-slip, (2) frequent fluctuations of temperature with micro-rupturing of the jog area and rupture propagation, and (3) pulses of temperature rising by stress accumulation near the fault tip and release by propagating ruptures.

Our experimental results offer new possibilities for observations of fault activity in the field. In most cases, a fault usually appears as a stepping break zone or a band zone rather than a linear fracture. As faults begin to build up strain, it can be observed that the changing trends of the thermal field of two kinds of jog areas are opposite, which provides evidence for analysis of slip sense of faults and stress fields. It is possible to observe change of heating mechanisms and search for unstable precursors by analysing thermal images from satellite databases and temperature measurements obtained on the ground. We believe that choosing some faults and observing their thermal states and behaviour of temperatures at their special portions in the field can be a challenging, yet promising project.

ACKNOWLEDGMENTS

This work was supported by the National Natural Science Foundation of China, grants 40872129 and 40572125. CHEN Guo-Qiang and HU Xiao-Yan participated in the experimental study. Discussions with GAO Xiang-Lin, CHEN Shun-Yun and MA Shengli have been useful for this work.

REFERENCES

Горький В.И. и др. Уходящее инфракрасное излучение Земли – индикатор сейсмической активности // Доклады АН СССР. – 1988. – Т. 301, № 1. – С. 67–69.

Ouzounov D., Freund F. Mid-infrared emission prior to strong earthquakes analyzed by remote sensing data // Advances in Space Research. – 2004. – V. 33. – P. 268–273.

Morzova L.I. Dynamics of Cloud Anomalies above Faults in Periods of Natural and Induced Seismicity // Izvestiya, Physics of the Soild Earth. – 1997. – V. 33, № 9. – P. 778–779.

Morzova L.I. Satellite meteorological images as carriers of information on seismic processes // Geology of Pacific Ocean. – 2000. – V. 15. – P. 439–446.

Tronin A.A. Satellite thermal survey – a new tool for the studies of seismoactive regions // International journal of remote sensing. – 1996. – V. 17. – P. 1439–1455.

Tronin A.A., Hayakawa M., Molchanov O.A. Thermal IR satellite data application for earthquake research in Japan and China // Journal of Geodynamics. – 2002. – V. 33. – P. 519–534.

Nusipov E., Abakanov T., Ospanov A.B., Ospanov A.M. Lugovskoe earthquake May 23, 2003 // The Fifth Kazakhstan-Chinesse IEnternaitonal Symposium: Modern Geodynamics and Seismic Risk of Central Asia. Almaty, September 24–27, 2003 – Almaty, 2003. – P. 17–18.

Tramutoli V. et al. TIR Satellite Techniques for monitoring the Earthquake active regions: review of the limits, achievements and perspectives // Fall Meeting, AGU, EOS, Nov. 7. 2004, T53C-06.

Chen M.H., Deng Z.H., Jia Q.H. The relationship between the satellite infrared anomalies before earthquake and the seismogenic fault-A case study on the 2001 Kunlun earthquake // Seismology and Geology. – 2003. – V. 25, № 1. – P. 100–108 (in Chinese).

Shan X.J., Qu C.Y., Ma J. Satellite thermal infrared observation and analysis on alternate activity of different segments of seismogenic fault // Journal of Geodesy and Geodynamics. – 2005. – V. 25, № 2. – P. 58–62 (in Chinese).

Ma J., Shan X.J. An attempt to study fault activity using remote sensing technology – A case of the Mani earthquake // Seismology and Geology. – 2000. – V 22, № 3. – P. 210–215 (in Chinese).

Lockner D.A.,,Okubo P.G. Measurements on Frictional Heating in Granite // Journal of Geophysical Research. – 1983. – V. 88, № B5. – P. 4313–4320.

Cui C.Y., Deng M.D., Geng N.G. Study on the features of spectrum radiation of rocks under different loading // Chinese Science Bulletin. – 1993. – V. 38, № 6. – P. 538–541 (in Chinese).

Deng M.D., Geng N.G., Cui C.Y. The study on the variation of thermal state of rocks caused by variation of stress state of rocks //

Earthquake Research in China. – 1997. – V. 13, № 2. – P. 179–185 (in Chinese).

Dong Y.F., Wang L.G., Liu X.F. et al. The experimental research of the infrared radiation in the process of rock deformation // Rock and Soil Mechanics. – 2001. – V. 22, № 2. – P. 134–137 (in Chinese).

Geng N.G., Cui C.Y., Deng M.D. Remote sensing detection of rock fracturing experiment and the beginning of remote rock mechanics // Acta Seismologica Sinica. – 1992. – V. 14 (Suppl.). – P. 645–652 (in Chinese).

Geng N.G., Cui C.Y., Deng M.D. et al. Remote sensing rock mechanics and its application prospects // Progress in Geophysics. – 1993. – V. 8, № 4. – P. 1–7 (in Chinese).

Wu L.X., Wang J.Z. Features of infrared thermal image and radiation temperature of coal rocks loaded. Science in China (Ser D). – 1998. – V. 28, № 1. – P. 41–46 (in Chinese).

Liu S.J., Wu L.X., Wu Y.H. et al. Analysis of affecting factors and mechanics of infrared radiation coming from loaded rocks // Mine Surveying. – 2003. – V. 3. – P. 67–70 (in Chinese).

Qian J.D., Deng M.D., Yin J.Y. et al. A basic experimental study of earthquake prediction in terms of radar technology // Chinese Journal of Geophysics. – 2005. – V. 48, № 5. – P. 1103–1109 (in Chinese).

Yin J.Y., Fang Z.F., Qian J.D. et al. Research on the application of infrared remote sensing in earthquake prediction and its physical mechanism // Earthquake Research in China. – 2000. – V. 16, № 2. – P. 140–148 (in Chinese).

Wu L.X., Liu S.J., Wu Y.H. et al. Precursors for rock fracturing and failure – Part I: IRR image abnormalities // International Journal of Rock Mechanics & Mining Sciences. – 2006. – V. 43. – P. 473–482.

Lixin Wu, Shanjun Liu, Yuhua Wu et al. Precursors for rock fracturing and failure – Part II: IRR *T*-Curve abnormalities // International Journal of Rock Mechanics & Mining Sciences. – 2006. – V. 43. – P. 483–493.

Freund F. Time-resolved study of charge generation and propagation in igneous rocks // Journal of Geophysical Research. – 2000. – V. 105, № B5. – P. 11001–11019.

Freund F. Charge generation and propagation in igneous rocks // Journal of Geodynamics. – 2002. – V. 33. – P. 543–570.

Freund F. On the electrical conductivity structure of the stable continental crust // Journal of Geodynamics. – 2003. – V. 35. – P. 353–388.

Freund A.A., Takeuchi A., Lau B.W.S. Stimulated infrared emission from rocks: assessing a stress indicator // eEarth Discuss. – 2006. – V. 1. – P. 97–121.

Liu P.X., Liu L.Q., Chen S.Y. et al. An experiment on the infrared radiation of surficial rocks during deformation // Seismology and Geology. – 2004. – V. 26, № 3. – P. 502–511 (in Chinese).

Liu Peixun, Ma Jin, Liu Liqiang, Ma Shengli, Chen Guoqiang. An experimental study on variation of thermal fields during the deformation of a compressive en echelon fault set // Progress in Natural Science. – 2007. – V. 17, № 3. – P. 298–304 (in Chinese).

Ma Jin, Liu Li-Qiang, Liu Pei-Xun et al. Thermal precursory pattern of fault unstable sliding: An experimental study of en echelon faults // Chinese Journal of Geophysics. – 2007. – V. 50. № 4. – P. 995–1004.

Chu T.C., Ranson W.F., Sutton M.A. et al. Applications of Digital Image Correlation Techniques to Experimental Mechanics // Experimental Mechanics. – 1985. – V. 25. – P. 232–244.

Jin Guanchang, Ma Shaopeng, Pan Yishan. Analysis of localization in rock materials through DSCM // Proceedings. SPIE, – 2002. – 4537. – P. 103–106.

Ma S., Wang L., Jin G. Damage evolution inspection of rock using digital speckle correlation method // Key Engineering Materials. – 2006. – V. 326–328. – P. 1117–1120.

Xie Ruisheng. Principles of Thermodynamics (M). – Beijing: People Education Press, 1980 (in Chinese).

Ma Jin
Institute of Geology,
Earthquake Administration,
100029, Beijing, China

Liu Liqiang
Institute of Geology,
Earthquake Administration,
100029, Beijing, China

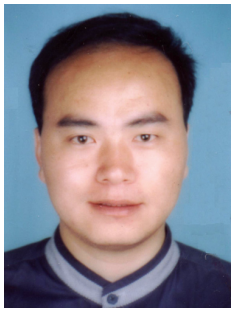

Ma Shaopeng
Beijing Institute of Technology,
100081, Beijing, China

Liu Peixun
Institute of Geology,
Earthquake Administration
100029, Beijing, China